Tailoring tunnel magnetoresistance by ultrathin Cr and Co interlayers: A first-principles investigation of Fe/MgO/Fe junctions

Peter Bose,[1,2] Peter Zahn,[1] Jürgen Henk,[3] and Ingrid Mertig[1,3]
[1]*Institute of Physics, Martin Luther University Halle-Wittenberg, Halle, D-06099 Saale, Germany*
[2]*International Max Planck Research School for Science and Technology of Nanostructures, Weinberg 2, Halle, D-06120 Saale, Germany*
[3]*Max Planck Institute of Microstructure Physics, Weinberg 2, Halle, D-06120 Saale, Germany*
(Received 16 February 2010; revised manuscript received 22 June 2010; published 13 July 2010)

We report on systematic *ab initio* investigations of Co and Cr interlayers embedded in Fe(001)/MgO/Fe(001) magnetic tunnel junctions, focusing on the changes in the electronic structure and the transport properties with interlayer thickness. The results of spin-dependent ballistic transport calculations reveal options to specifically manipulate the tunnel magnetoresistance ratio. The resistance-area products and the tunnel magnetoresistance ratios show a monotonous trend with distinct oscillations as a function of the Cr thickness. These modulations are directly addressed and interpreted by means of magnetic structures in the Cr films and by complex band-structure effects. The characteristics for embedded Co interlayers are considerably influenced by interface resonances which are analyzed by the local electronic structure.

DOI: 10.1103/PhysRevB.82.014412 PACS number(s): 75.47.−m, 72.25.Mk, 73.22.−f, 73.40.Gk

I. INTRODUCTION

During the last years, magnetoresistive effects—in particular, the tunnel magnetoresistance (TMR) effect[1,2]—became increasingly important for the fast developing field of spintronic devices.[3,4] The first industrial applicable TMR contacts have been built using crystalline MgO insulators which are epitaxially grown on as well as coated with iron electrodes.[5,6] Fe/MgO/Fe magnetic tunnel junctions (MTJs) have been extensively investigated to elucidate the mismatch between theoretically predicted[7,8] and the at least one order of magnitude smaller measured[9,10] TMR ratios. It turned out that the disparity can be attributed to differences between idealized (in theory) and real (in experiment) samples. More sophisticated theories which include imperfections, such as interface disorder[11–17] or roughness effects,[18] were able to close the gap between experiment and theory and highlight the importance of perfect interfaces.

Although other tunnel junctions, such as CoFeB/MgO/CoFeB MTJs with their high TMR ratios,[19] were put into the focus of attention, Fe/MgO/Fe MTJs are still intensely studied. Besides the emerging field of spin-torque effects,[20] research is ongoing in search of other ways to increase the TMR ratio further. Instead of improving the interface quality an alternative means is found in the specific manipulation of the spin-dependent conductances by embedding ultrathin interlayers.[21,22]

The insertion of a single layerwise antiferromagnetic (LAFM) Cr interlayer results into even-odd oscillations of the TMR ratio as a function of the Cr thickness.[23,24] In this paper, we report on a first-principles study of these transport characteristics. We discuss the origin of these modulations with the apparent 2 monolayer (ML) wavelength as well.

Additionally, an analysis of the electronic-transport results for Co interlayers at both Fe/MgO interfaces is presented. These investigations were motivated by previous *ab initio* calculations[25] which predicted larger TMR ratios for MgO tunnel junctions with bcc Co(001) leads instead of Fe(001) electrodes. Due to the fact that Co grows epitaxially only up to a few monolayers on bcc substrates, a question arises whether ultrathin Co interlayers could be alternatively used to obtain an enhancement of the TMR ratios in Fe/MgO/Fe MTJs. To answer this question we computed the conductances and TMR ratios for small Co interlayer thicknesses and analyzed the results by means of the electronic structures.

II. THEORETICAL BACKGROUND

Our computational approach is divided into two steps. First, the electronic structures of the MTJs are calculated from first principles. Second, the electronic-transport properties are computed, using the potentials obtained in the first step.

The electronic structure is determined self-consistently within the framework of density-functional theory using a scalar-relativistic screened Korringa-Kohn-Rostoker Green's-function technique.[26,27] The spherical site potentials were treated in the atomic sphere approximation (ASA) using the local spin-density approximation for the exchange-correlation potential.[28] Throughout this work, a parameterization following Vosko *et al.*[29] was used.

Since structural information of Fe/MgO/Fe MTJs with embedded ultrathin Cr and Co spacers are not reported so far, we resort to a geometry of planar Fe(001)/MgO/Fe(001) junctions which has been used in previous theoretical studies.[16,30] Here, the bulk bcc Fe layers are fixed at the experimental lattice constant of 2.866 Å. The fcc MgO in-plane lattice constant is chosen larger than that of the Fe by a factor of $\sqrt{2}$.[7] The interlayer distances were taken from surface x-ray diffraction analyses for a thin MgO film on Fe(001).[31,32] In detail, a supercell geometry with six MgO layers sandwiched by 20 Fe layers was used to compute self-consistently the atomic potentials ($\ell_{\max}=3$). The insertion of x magnetic atomic layers in planar Fe(001)/x(Cr)/6(MgO)/Fe(001) and Fe(001)/x(Co)/6(MgO)/x(Co)/Fe(001) junctions was achieved by replacing x Fe MLs at the Fe/MgO interfaces by x Cr or Co layers.

This procedure implies that Cr and Co atoms occupy the same positions as the replaced Fe atoms; worded differently, the interlayers follow the bcc structure of the Fe(001) leads.

Due to the broken translational invariance in transport direction (z, i.e., [001]) and the in-plane translational invariance, the eigenstates of the electrodes are labeled by in-plane wave vectors $\boldsymbol{k}_\parallel=(k_x,k_y)$. The point group of the two-dimensional lattice is $4mm$.

The ballistic conductance C per unit cell area $A_\square$ is computed for zero-bias voltage in terms of transmission probabilities (Landauer-Büttiker approach[33]) at the Fermi energy E_F,

$$C=\frac{e^2}{h}\int_{2\mathrm{BZ}} T(\boldsymbol{k}_\parallel,E_F)d\boldsymbol{k}_\parallel. \tag{1}$$

The transmission probability $T(\boldsymbol{k}_\parallel,E_F)$ is obtained by means of a Green's-function approach.[34] The integration over the two-dimensional Brillouin zone (2BZ) requires typically about 90 000 $\boldsymbol{k}_\parallel$. The use of special $\boldsymbol{k}_\parallel$ points[35] reduces that number to 1/8. The resistance-area product

$$RA=\frac{1}{C}, \tag{2}$$

as normalized quantity, is used to compare the theoretical with experimental data.

The optimistic TMR ratio is obtained from the RA's which are computed for the parallel (P) and the antiparallel (AP) alignment of the two Fe(001) lead magnetizations,

$$\mathrm{TMR}=\frac{RA^{\mathrm{AP}}-RA^{\mathrm{P}}}{RA^{\mathrm{P}}}. \tag{3}$$

For the normalized TMR ratio, the denominator is replaced by $RA^{\mathrm{AP}}+RA^{\mathrm{P}}$. Since interfaces determine considerably the transport properties, transmittance maps which display $T(\boldsymbol{k}_\parallel,E_F)$ versus $\boldsymbol{k}_\parallel$ need to be interpreted by means of the local electronic structure, rather than by the electronic structures of the bulk electrodes. The former is obtained from the layer-resolved Bloch spectral density,

$$N_{al}(E,\boldsymbol{k}_\parallel)=-\frac{1}{\pi}\mathrm{Im\ Tr}\ G^{+}_{al}(E,\boldsymbol{k}_\parallel), \tag{4}$$

of atom a in layer l. $G^{+}_{al}(E,\boldsymbol{k}_\parallel)$ is the site-diagonal Green's function of that site. The trace involves integration over the ASA sphere and summation over spin-angular quantum numbers.

III. RESULTS

A. Cr interlayer in Fe(001)/MgO/Fe(001)

In the following, we present results of the thickness dependence of both the conductances and the TMR ratios for ultrathin Cr interlayers which are embedded at a single interface in Fe(001)/x(Cr)/6(MgO)/Fe(001) MTJs. The Cr thickness d_{Cr} is varied in steps of MLs, $x=0,\ldots,7$ with $d_{\mathrm{Cr,1\ ML}}=2.35$ Å, $d_{\mathrm{Cr,2\ ML}}=4.04$ Å, and $d_{\mathrm{Cr},x\ \mathrm{ML}}=d_{\mathrm{Cr,2\ ML}}+x\cdot 1.69$ Å.

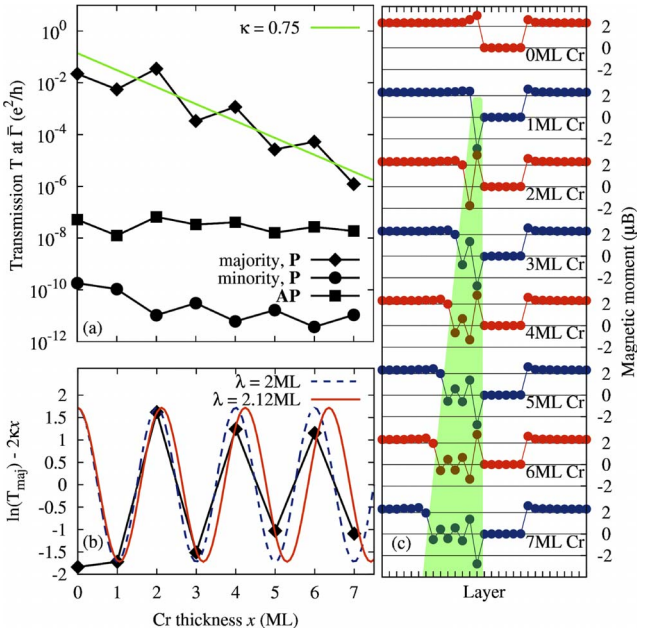

FIG. 1. (Color online) (a) Dependence of spin-resolved P (majority, minority) and AP transmissions on a logarithmic scale versus Cr thickness x for Bloch states at $\boldsymbol{k}_\parallel=0$ in Fe(001)/x(Cr)/6(MgO)/Fe(001) MTJs, $x=0,\ldots,7$. The green solid line is a fitted exponential to the majority transmission. The deviation of the majority transmission from this fit is shown in panel (b). These data are fitted by cosine functions (fixed at $x=1$) with 2 ML (dashed, blue) and 2.17 ML (solid, red) periods. (c) Magnetic profiles of MTJs with Cr layer thicknesses $x=0,\ldots,7$ ML. The transparent green area highlights the magnetic moments of the Cr layers.

We start with the tunneling behavior of Bloch states at $\bar{\Gamma}(\boldsymbol{k}_\parallel=0)$. The associated transmission probabilities for $x=0,\ldots,7$ are plotted in Fig. 1(a). Both the minority-spin contribution for P and the AP contribution stay almost constant whereas the majority-spin contribution of P decays exponentially with an oscillatory modulation. Its decay rate is estimated by an exponential fit, $\exp(-2\kappa x)$ with $\kappa=0.75$ [green solid line in Fig. 1(a)].

It turns out that an oscillatory modulation of $T^{\mathrm{P}}_{\mathrm{maj}}$ shows up for all $\boldsymbol{k}_\parallel$ within the 2BZ. These oscillations are also present in the conductance C which is an integral over the transmission probabilities, Eq. (1); hence, there is no destructive interference which would lead to (complete) cancellation. Thus, it is essential to elucidate the underlying mechanism of these oscillations. To strengthen the discussion, we focus in the following on the transmissions at $\bar{\Gamma}$.

The oscillation period can be estimated by fitting cosine functions to the deviation of $T^{\mathrm{P}}_{\mathrm{maj}}(\boldsymbol{k}_\parallel=0)$ from the averaged exponential decay [black diamonds in Fig. 1(b)]. The fit with a period of 2 ML (blue) reproduces only the peak positions but deviates significantly in amplitude. A second fit, with 2.17 ML period (red), hits the data best.

A 2 ML oscillation might be attributed to the local magnetic structure of the LAFM Cr interlayers [Fig. 1(c)]. The magnetic moments of the Cr layers at the Cr/MgO interface are sizably enhanced due to the nonmagnetic MgO film.

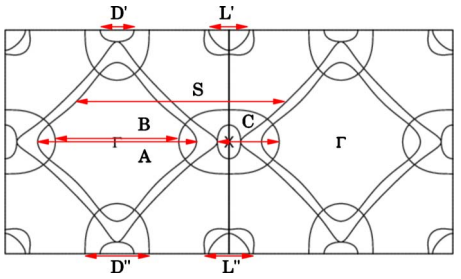

FIG. 2. (Color online) Fermi-surface cross sections in the (100) plane of c-afm Cr. The nesting vectors along [001] (arrows) are shown in an extended zone scheme and are listed in Table I.

Within a simple model, one could think of the LAFM Cr films as quasi-one-dimensional, with spin-dependent (alternating) Kronig-Penney potential landscapes.[36] It is reasonable to assume that the partially uncompensated Cr magnetic moments at the MgO interface would induce a lowering of the associated potential steps for one spin species and a lifting for the other one. Consequently, electrons propagate differently in dependence on their spin. The Cr interface layers act therefore as spin filters for the tunneling currents. Hence, the latter are increased (decreased) if the magnetic moments within the Cr interface layers are parallel (antiparallel) to the magnetization of the opposite Fe electrode. Due to the LAFM growth of the Cr interlayer, the tunnel current characteristics should exhibit signatures of 2 ML oscillations. The maxima of these oscillations should arise for P (AP) magnetic configurations of the Fe leads at even (odd) multiples of the Cr interlayer thickness x. This behavior was already found for LAFM Mn interlayers in Fe(001)/x(Mn)/Vac/Fe(001) MTJs.[37] However, the mismatch in Fig. 1(b) appears like an undersampling which cannot be satisfactorily explained by means of the spin-filter effect. The better match of the other oscillation period with 2.17 ML points to another effect which additionally influences the electronic transport.

There are two possible mechanisms that may explain other wavelengths than the 2 ML. First, one could think of spin-density waves within the Cr interlayers. Spin-density waves are found for Cr bulk systems[38] and are related to nesting vectors of the Fermi surface. Nesting vectors that come into question are shown in Fig. 2 for a cross section of the Fermi surface in the (100) plane. The corresponding wavelengths of these vectors along the [001] direction (i.e., in transport and growth direction) are given in Table I. The only vector that exhibits a wavelength which is comparable to that of the transmission (2.17 ML) is S, with an oscillation period of 2.12 ML. However, since we are interested in the oscillatory onset at $\boldsymbol{k}_{\parallel}=0$, the vector S cannot explain our findings because it is offset from $\bar{\Gamma}$.

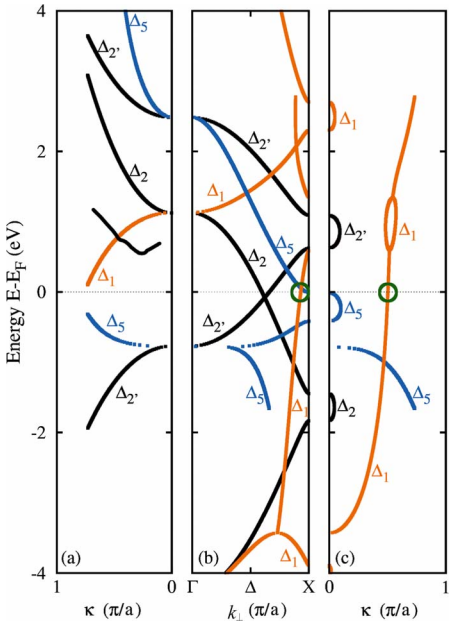

FIG. 3. (Color online) Complex band structure of bulk bcc Cr in the c-afm phase along [001] for $\boldsymbol{k}_{\parallel}=0$. The real part of $k_{\perp}$ and the exponential decay rate κ (imaginary part of $k_{\perp}$) are shown in panels (b) and (a), (c), respectively. The color code of the bands indicates the irreducible representations of the point group $4mm$ of the associated Bloch states. The green circles at the Fermi energy mark the complex Δ_1 band, to $k_{\perp}=(0.922,0.503)\frac{\pi}{a}$, which governs the transmission of majority electrons at $\bar{\Gamma}$ [cf. Fig. 1(a)].

The oscillatory exponential decay of $T^{\mathrm{P}}_{\mathrm{maj}}(\boldsymbol{k}_{\parallel}=0)$ is explained most promisingly in terms of the complex band structure[39] of the Cr interlayers. Since a (continuous) dispersion relation is not defined for thin films, due to lack of translational invariance, we refer to the complex band structure of bulk Cr along [001]. The latter is decomposed with respect to the irreducible representations of the point group $4mm$ (Δ_1, Δ_5, Δ_2, and $\Delta_{2'}$) of the associated Bloch states (Fig. 3).

A complex band structure of a periodic system is the conventional band structure extended to Bloch vectors $(\boldsymbol{k}_{\parallel},k_{\perp})$ with complex wave numbers $k_{\perp}$. The associated bands can be cast into four categories:[40] (i) *real bands* which correspond to the conventional band structure and have Im $k_{\perp}=0$; (ii) *imaginary bands of the first kind* have Re $k_{\perp}=0$ and Im $k_{\perp}\neq 0$; (iii) *imaginary bands of the second kind* with Re $k_{\perp}=\frac{\pi}{a}$ and Im $k_{\perp}\neq 0$; and (*iv*) *complex bands* with Re $k_{\perp}\neq 0$, Re $k_{\perp}\neq\frac{\pi}{a}$, and Im $k_{\perp}\neq 0$.

The imaginary part of $k_{\perp}$ is denoted as κ and represents a measure for the decay rate of the evanescent wave function.[41] At the Fermi energy, a complex band of the second kind shows up at $k_{\perp}=(0.922,0.503)\frac{\pi}{a}$ (circles in Fig. 3).

TABLE I. Nesting vectors of commensurate AFM (c-afm) Cr along [001], as given in Fig. 2, are characterized by their oscillation periods (in ML).

c-afm	L′	L″	S	A	B	C	D′	D″
λ (ML)	11.03	9.21	2.12	2.82	3.62	7.21	13.26	6.96

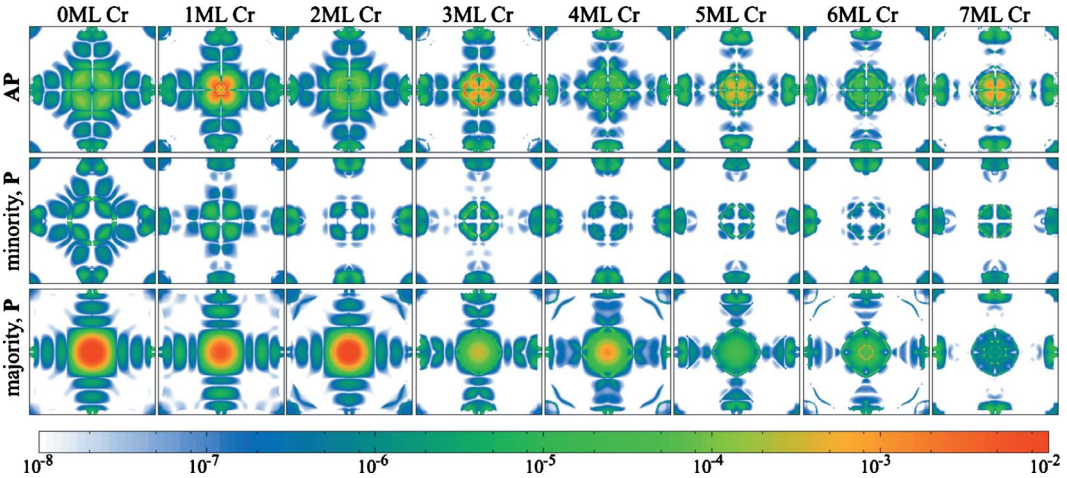

FIG. 4. (Color online) Majority (P, bottom row), minority (P, middle row), and AP (top row) transmission $T(\boldsymbol{k}_\parallel, E_F)$ within two-dimensional Brillouin zones for Fe(001)/x(Cr)/6(MgO)/Fe(001) MTJs with Cr layer thicknesses of $x=0,\ldots,7$ ML (from left to right). The two-dimensional Brillouin zones cover the range between $-\pi/a$ and π/a.

The corresponding decay rate of $\kappa=0.78/\mathrm{ML}$ matches well the estimated exponential decay of the majority transmission [$\kappa=0.75/\mathrm{ML}$, Fig. 1(a)]. Due to the nonvanishing real part, the exponential decay exhibits an oscillatory envelope with a wavelength $\lambda=\frac{\pi}{\mathrm{Re}[k_\perp]}\approx 2.17$ ML which agrees well with the fit in Fig. 1(b). We conclude therefore that the thickness dependence of the transmission for the majority states at the $\bar{\Gamma}$ point is very likely governed by this Δ_1 state, provided the electronic structure of ultrathin Cr films is well described by that of bulk Cr. The latter is presumably the case for Cr thicknesses of $x\geq 4$ ML.[42] Surprisingly, we observe that the found κ for these thick interlayers, even describes very well the exponential decay for thinner Cr thicknesses [Fig. 1(a)].

Transmission maps display the spin-resolved transmission for P and AP versus $\boldsymbol{k}_\parallel$ for each Cr thickness x (Fig. 4). As observed for $T^{\mathrm{P}}_{\mathrm{maj}}(\boldsymbol{k}_\parallel=0)$, one finds within the majority transmission maps a clearly visible modulation of $T^{\mathrm{P}}_{\mathrm{maj}}(\boldsymbol{k}_\parallel)$ for $\boldsymbol{k}_\parallel$ points in the center regions with maxima (minima) at even (odd) multiples of x. It is reasonable to assume that the oscillations of these transmissions are caused by the same band-structure effect as it was discussed for $T^{\mathrm{P}}_{\mathrm{maj}}$ at $\bar{\Gamma}$. Furthermore, the majority *RA* products in Fig. 5 exhibit even-odd oscillations as well, indicating constructive superposition of the oscillations of the individual $T^{\mathrm{P}}_{\mathrm{maj}}(\boldsymbol{k}_\parallel)$.

Although the cloverleaflike structures within the minority transmission maps in Fig. 4 exhibit slight variations which are in antiphase to the majority transmission modulations, the corresponding *RA* products in Fig. 5 reveal no signatures of such an even-odd characteristic. The weak thickness dependence can be understood with help of the complex band structure in Fig. 3. From first-principles investigations on Fe/MgO/Fe it is known[43,44] that Δ_5 states are the main carrier within the minority transport channel. Due to the Δ_5 *real band* at the Fermi energy, it is very likely that these Bloch states just propagate undamped through the Cr interlayer. The minority *RA* is therefore marginally affected by the Cr spacer and gives contributions which are similar to those of Fe/MgO/Fe MTJs.

In contrast to the above finding, the pronounced modulations within the AP transmission maps in Fig. 4—with maxima (minima) at odd (even) x—lead to an even-odd oscillation of the corresponding *RA*. Due to the spin-filter effect of the Cr interface layer RA^{AP} is in antiphase to $RA^{\mathrm{P}}_{\mathrm{maj}}$.

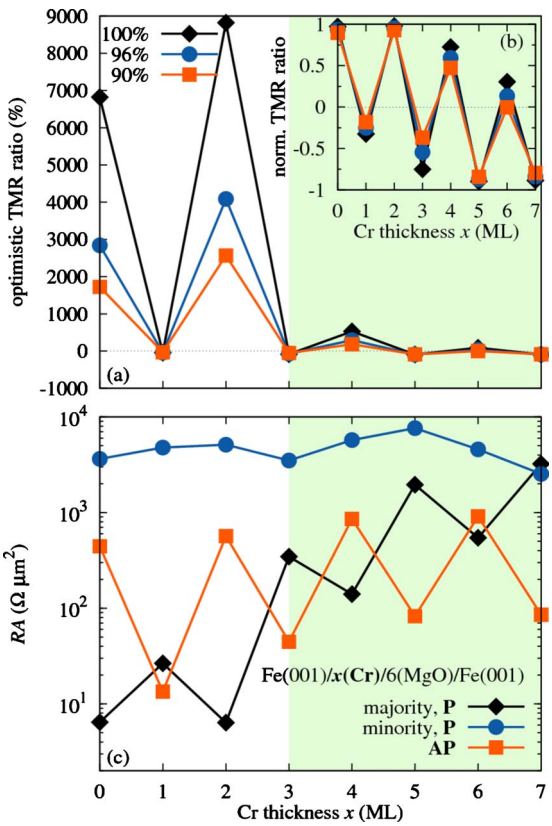

FIG. 5. (Color online) Cr-thickness dependence of (a) optimistic and (b) normalized TMR ratios in Fe(001)/x(Cr)/6(MgO)/Fe(001) MTJs. Since variations in the Cr layer thickness cannot be ruled out in experiment, a model with resistors in parallel connection is assumed to mimic Cr-thickness fluctuations (line styles indicate the weight w; see text). (c) Resistance-area product *RA* for parallel magnetic (P: majority, minority) and antiparallel magnetic configurations (AP), shown on a logarithmic scale.

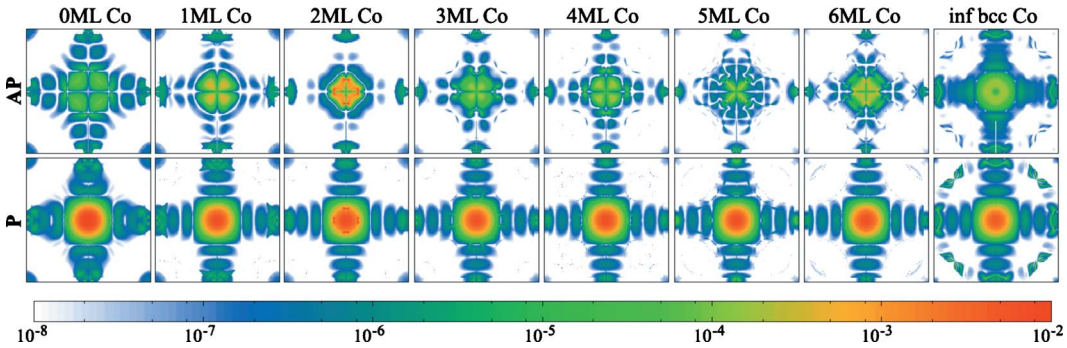

FIG. 6. (Color online) Transmission $T(\boldsymbol{k}_{\parallel}, E_F)$ for the P (bottom row) and AP (top row) magnetic configuration within two-dimensional Brillouin zones for Fe(001)/x(Co)/6(MgO)/x(Co)/Fe(001) MTJs, $x=0,\ldots,6$ ML (from left to the right). The panels on the right-hand side are for Co(001)/6(MgO)/Co(001) MTJs with infinite bcc Co leads. The Brillouin zones cover the range between $-\pi/a$ and π/a.

This behavior results in TMR ratios which exhibit 2 ML oscillations with periodic changes in the sign. The amplitudes of the TMR ratios, are with about 7000% and 9000% at $x=0$ and 2 ML, considerably larger than for the other thicknesses, with values between about −100% and +100%. This even-odd oscillation of the TMR ratio as a function of the Cr thickness has been observed experimentally[24] but with a phase shift of 1 ML. In more recent experiments,[45] it has been found that this phase shift depends on whether the Cr interlayer is grown after or before growth of the MgO barrier. However, a large maximum of the TMR ratio for small Cr thicknesses does not show up in both growth conditions. Instead, an exponential decay of the optimistic TMR ratio for increasing x is reported.[24] Since variations in the Cr layer thickness cannot be ruled out in experiment, we assume a model with resistors in parallel connection to mimic Cr-thickness fluctuations. The resistance of the mean thickness x is weighted by w, the contributions from $x-1$ and $x+1$ are weighted by $(100\%-w)/2$, respectively. With already large central weights of $w=96\%$ and $w=90\%$, this model is able to reproduce the principal experimental TMR characteristics.[24] For a detailed analysis of the effect of structural imperfections, however, one has to rely on more sophisticated computational approaches, such as the coherent-potential approximation or a supercell method.

B. Fe(001)/x(Co)/6(MgO)/x(Co)/Fe(001)

In this section, we discuss the effects of Co interlayers embedded into Fe(001)/MgO/Fe(001) MTJs on the electronic transport. With respect to previous theoretical investigations of MgO barriers with bcc Co leads,[25] we specifically studied the thickness dependence of ultrathin Co interlayers which are inserted at *both* Fe/MgO interfaces. Since Co grows epitaxially only up to few monolayers on a bcc substrate, the Co thicknesses d_{Co} are restricted to $x \leq 6$ ML. The monolayer separations are taken identical to the case of Cr interlayers. Substituting all Fe atoms with Co atoms the effect of semi-infinite bcc Co leads is studied in addition.

First, we recall previously reported conductances and TMR ratios in MTJs with equal thicknesses of both Co interlayers.[46] The corresponding $\boldsymbol{k}_{\parallel}$-resolved transmissions versus x are shown in Fig. 6 for both magnetic configurations (P, AP). The shapes of the transmission maps for P configuration (bottom row) are—beside the case of the semi-infinite Co leads—very similar. In contrast to this weak dependence, one observes a rise and a decline of the transmission probabilities in the central regions of the Brillouin zones for the AP configuration for small x (top row). The maximum shows up at $x=2$ ML. Based on these observations, it is reasonable to expect a relatively constant behavior of the P conductance and a maximum at $x=2$ ML for the AP conductance.

The elsewhere published conductances and TMR ratios[46] are inserted into Fig. 7 as red boxes. In accordance with the findings for bcc Co leads,[25] we identify specific Co thicknesses ($x=3$ and 5 ML) that exhibit larger TMR values than those obtained for pure Fe/MgO/Fe junctions. In particular, the TMR ratio follows the even-odd-type characteristic which shows up for the conductance C^{P}. But this behavior of C^{P} does not reflect the weak thickness dependence as expected from the transmission probabilities (Fig. 6). It turned out that this even-odd change is considerably affected by single interface resonances whose transmission probabilities contribute with up to 70% to the conductance.[47] These hot spots within the transmission maps occur preferably in ideal, symmetric MTJs at zero-bias voltage.[21] They are strongly diminished by breaking the symmetry, for instance, by means of a tiny bias voltage or structural imperfections of the sample. A bias voltage of 0.02 V is sufficient to destroy the resonant states and to reduce the corresponding transmission probabilities by several orders of magnitude.

The total number of hot spots in each transmission map of Fig. 6 is less than 10. Instead of removing the resonances by a small bias voltage, the transmissions of these states are identified and neglected. These filtered data are shown as black diamonds in Fig. 7. The effect of the resonances shows up mainly for C^{P}. For the latter one obtains, after an initial decrease in about 50% from $x=0$ to 1 ML, the expected nearly constant behavior.

The filtered AP conductances agree well with unfiltered ones, in particular, the maximum at $x=2$ ML. Inspecting the corresponding transmission map (Fig. 6), this maximum is attributed to enhanced transmissions in the center region of the 2BZ which are caused by Δ_5-minority interface resonances within the Co interface layer [Fig. 7(d)]. In contrast to the transmission resonances (hot spots), these transmissions are unaffected by small bias voltages.

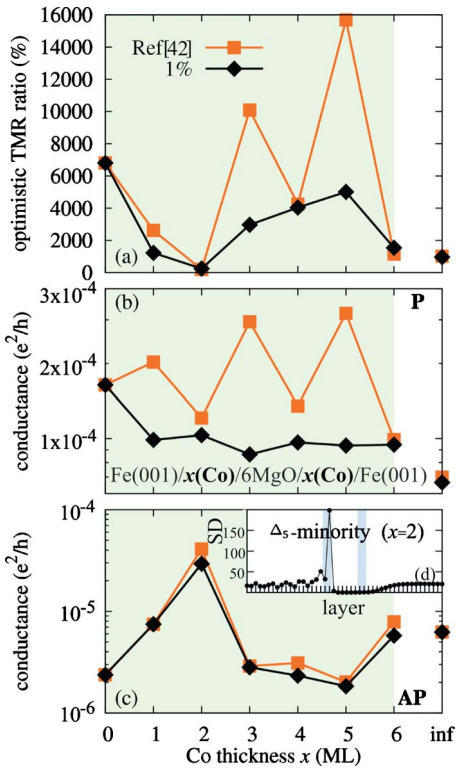

FIG. 7. (Color online) Co thickness dependence of (a) optimistic TMR ratio, (b) P, and (c) AP conductances in symmetric Fe(001)/x(Co)/6(MgO)/x(Co)/Fe(001) MTJs. Red squares, taken from Ref. 46, are for data which exhibit hot spots in the transmission probabilities $T(\boldsymbol{k}_\parallel, E_F)$. The black symbols show the data with these hot spots being removed (see text). Panel (d) displays the layer-resolved spectral density (in states/hartree) of a Δ_5-minority interface resonance with $\boldsymbol{k}_\parallel = (0.095, 0.008)\frac{\pi}{a}$. The blue areas mark the position of the 2-ML-thick Co interlayers within the MTJ.

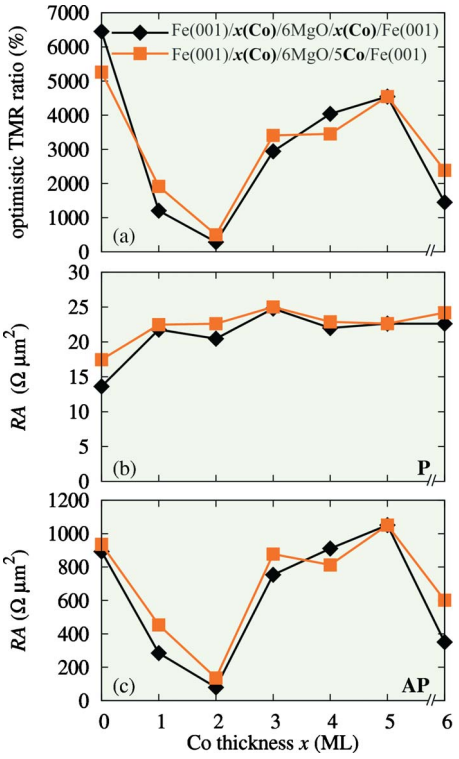

FIG. 8. (Color online) (a) Optimistic TMR ratios and resistance-area products RA for (b) P and (c) AP of symmetric (black) and asymmetric (red) Fe(001)/x(Co)/6(MgO)/y(Co)/Fe(001) MTJs. Hot spots were filtered out (see, e.g., Fig. 7).

Since the thickness dependence of C^{P} is weakened by the filter procedure, that of the TMR ratio is as well. In particular, the maxima at $x=3$ and 5 ML do not show up. The minimum of approximately 200% at $x=2$ ML is, however, still present; it is explained by the increase in C^{AP}—up to a value comparable with C^{P}—due to the Δ_5-minority interface resonances. For increasing x, the TMR ratio increases monotonously up to a maximum at $x=5$ ML, with 4600% considerably smaller than the 7000% obtained for pure Fe/MgO/Fe MTJs.

We note in passing that the enhanced TMR ratio in MTJs with semi-infinite bcc Co leads, reported in Ref. 25, are not reproduced. Previous investigations of Fe/MgO/Fe systems have shown that conductances depend strongly on details of the calculations, in particular, on the atomic positions in the interface region. Thus, one is lead to attribute the above-mentioned discrepancy to computational details.

Since increased TMR ratios are not obtained by symmetric MTJs, we studied the effect of asymmetric MTJs, with one interlayer thickness fixed to 5 ML, in addition. The fixed thickness of 5 ML is chosen with respect to the largest TMR ratio in symmetric MTJs (Fig. 7). Both the RA products and the TMR ratios of the asymmetric junctions do not differ significantly from those of the symmetric junctions (Fig. 8). For both kinds of MTJs, the TMR ratio follows the characteristics of RA^{AP} because RA^{P} is almost constant. The presence of the minimum at $x=2$ ML additionally substantiates that the Δ_5-minority interface resonances, which cause the drop of RA^{AP}, are marginally affected by symmetry breaking of an ideal MTJ.

IV. CONCLUSION

In summary, the computed conductances and TMR ratios exhibit the oscillatory decays with the thickness of ultrathin Cr interlayers, which have been found in experiment. The analysis of the associated transmission probabilities reveals that the tunneling of Bloch states is affected by the interplay of two mechanisms. On the one hand, a spin-filter effect which is induced by the enhanced magnetic moments of the Cr interface layers and on the other hand, the presence of complex bands which are formed within the Cr interlayers. The oscillations are therefore mixtures of 2 ML oscillations of magnetic origin and superpositions of the individual modulations of the tunneling Bloch states, which can be traced back to the corresponding complex wave vectors. Our results further indicate that spin-density waves are of minor importance for understanding of electronic transport through Fe/MgO/Fe MTJs with ultrathin Cr interlayers.

The embedding of Co interlayers at both interfaces does not lead to an increase in the TMR ratios with respect to Fe/MgO/Fe MTJs. Please note that the reference values for $x=0$ (i.e., no Co interlayer) have been calculated under the assumption of ideal interface structures and are therefore probably considerably overestimated. Thus, we suggest to include the effects of imperfect interfaces, which are unavoidable in real samples, in a future investigation.

ACKNOWLEDGMENTS

Helpful discussions with S. Yuasa, R. Matsumoto, and N. F. Hinsche are gratefully acknowledged. This work is supported by the Sonderforschungsbereich 762, Functionality of Oxidic Interfaces. P.B. is supported by the International Max Planck Research School for Science and Technology of Nanostructures.

[1] M. Julliere, Phys. Lett. A **54**, 225 (1975).
[2] J. S. Moodera, L. R. Kinder, T. M. Wong, and R. Meservey, Phys. Rev. Lett. **74**, 3273 (1995).
[3] I. Žutić, J. Fabian, and S. Das Sarma, Rev. Mod. Phys. **76**, 323 (2004).
[4] S. A. Wolf, A. Y. Chtchelkanova, and D. M. Treger, IBM J. Res. Dev. **50**, 101 (2006).
[5] W. J. Gallagher and S. S. P. Parkin, IBM J. Res. Dev. **50**, 3 (2006).
[6] S. Yuasa and D. D. Djayaprawira, J. Phys. D **40**, R337 (2007).
[7] W. H. Butler, X.-G. Zhang, T. C. Schulthess, and J. M. MacLaren, Phys. Rev. B **63**, 054416 (2001).
[8] J. Mathon and A. Umerski, Phys. Rev. B **63**, 220403 (2001).
[9] S. Yuasa, T. Nagahama, A. Fukushima, Y. Suzuki, and K. Ando, Nature Mater. **3**, 868 (2004).
[10] S. S. P. Parkin, C. Kaiser, A. Panchula, P. M. Rice, B. Hughes, M. Samant, and S.-H. Yang, Nature Mater. **3**, 862 (2004).
[11] X.-G. Zhang, W. H. Butler, and A. Bandyopadhyay, Phys. Rev. B **68**, 092402 (2003).
[12] J. Mathon and A. Umerski, Phys. Rev. B **74**, 140404 (2006).
[13] H. Itoh, J. Ozeki, and J. Inoue, J. Magn. Magn. Mater. **303**, e205 (2006).
[14] D. Waldron, V. Timoshevskii, Y. Hu, K. Xia, and H. Guo, Phys. Rev. Lett. **97**, 226802 (2006).
[15] C. Heiliger, P. Zahn, and I. Mertig, J. Magn. Magn. Mater. **316**, 478 (2007).
[16] P. Bose, A. Ernst, I. Mertig, and J. Henk, Phys. Rev. B **78**, 092403 (2008).
[17] F. Bonell, S. Andrieu, A. M. Bataille, C. Tiusan, and G. Lengaigne, Phys. Rev. B **79**, 224405 (2009).
[18] P. X. Xu, V. M. Karpan, K. Xia, M. Zwierzycki, I. Marushchenko, and P. J. Kelly, Phys. Rev. B **73**, 180402 (2006).
[19] S. Ikeda, J. Hayakawa, Y. Ashizawa, Y. M. Lee, K. Miura, H. Hasegawa, M. Tsunoda, F. Matsukura, and H. Ohno, Appl. Phys. Lett. **93**, 082508 (2008).
[20] R. Matsumoto *et al.*, Phys. Rev. B **80**, 174405 (2009).
[21] K. D. Belashchenko, J. Velev, and E. Y. Tsymbal, Phys. Rev. B **72**, 140404 (2005).
[22] F. Greullet, C. Tiusan, F. Montaigne, M. Hehn, D. Halley, O. Bengone, M. Bowen, and W. Weber, Phys. Rev. Lett. **99**, 187202 (2007).
[23] T. Nagahama, S. Yuasa, E. Tamura, and Y. Suzuki, Phys. Rev. Lett. **95**, 086602 (2005).
[24] R. Matsumoto, A. Fukushima, K. Yakushiji, S. Nishioka, T. Nagahama, T. Katayama, Y. Suzuki, K. Ando, and S. Yuasa, Phys. Rev. B **79**, 174436 (2009).
[25] X.-G. Zhang and W. H. Butler, Phys. Rev. B **70**, 172407 (2004).
[26] R. Zeller, P. H. Dederichs, B. Ùjfalussy, L. Szunyogh, and P. Weinberger, Phys. Rev. B **52**, 8807 (1995).
[27] N. Papanikolaou, R. Zeller, and P. H. Dederichs, J. Phys.: Condens. Matter **14**, 2799 (2002).
[28] W. Kohn and L. J. Sham, Phys. Rev. **140**, A1133 (1965).
[29] S. H. Vosko, L. Wilk, and M. Nusair, Can. J. Phys. **58**, 1200 (1980).
[30] C. Heiliger, P. Zahn, B. Y. Yavorsky, and I. Mertig, Phys. Rev. B **72**, 180406 (2005).
[31] H. L. Meyerheim, R. Popescu, N. Jedrecy, M. Vedpathak, M. Sauvage-Simkin, R. Pinchaux, B. Heinrich, and J. Kirschner, Phys. Rev. B **65**, 144433 (2002).
[32] C. Tusche, H. L. Meyerheim, N. Jedrecy, G. Renaud, A. Ernst, J. Henk, P. Bruno, and J. Kirschner, Phys. Rev. Lett. **95**, 176101 (2005).
[33] Y. Imry and R. Landauer, Rev. Mod. Phys. **71**, S306 (1999).
[34] J. Henk, A. Ernst, K. K. Saha, and P. Bruno, J. Phys.: Condens. Matter **18**, 2601 (2006).
[35] R. A. Evarestov and V. P. Smirnov, Phys. Status Solidi B **119**, 9 (1983).
[36] U. Schlickum, C. L. Gao, W. Wulfhekel, J. Henk, P. Bruno, and J. Kirschner, Phys. Rev. B **74**, 054409 (2006).
[37] P. Bose, I. Mertig, and J. Henk, Phys. Rev. B **75**, 100402 (2007).
[38] E. Fawcett, Rev. Mod. Phys. **60**, 209 (1988).
[39] V. Heine, Phys. Rev. **138**, A1689 (1965).
[40] Y.-C. Chang, Phys. Rev. B **25**, 605 (1982).
[41] Since $k_\perp$ is commonly defined in units of $\frac{\pi}{a}$ and a corresponds to an interlayer distance of 2 ML, a factor of $\frac{\pi}{2}$ has to be incorporated to obtain it in units of $\frac{1}{\mathrm{ML}}$.
[42] C. M. Schneider, P. Schuster, M. Hammond, H. Ebert, J. Noffke, and J. Kirschner, J. Phys.: Condens. Matter **3**, 4349 (1991).
[43] C. Heiliger, P. Zahn, and I. Mertig, Mater. Today **9**, 46 (2006).
[44] W. H. Butler, Sci. Technol. Adv. Mater. **9**, 014106 (2008).
[45] R. Matsumoto and S. Yuasa (private communication).
[46] P. Bose, P. Zahn, J. Henk, and I. Mertig, *Novel Materials and Devices for Spintronics*, edited by O. G. Heinonen, S. Sanvito, V. A. Dediu, and N. Rizzo, MRS Symposium Proceedings No. 1183 (Materials Research Society, Pittsburgh, 2009), 1183-FF07-2.
[47] O. Wunnicke, N. Papanikolaou, R. Zeller, P. H. Dederichs, V. Drchal, and J. Kudrnovsky, Phys. Rev. B **65**, 064425 (2002).